

Variable location channels to improve efficiency and precision for direct ∇T_e measurements and high spatial resolution T_e -profile measurements using electron cyclotron emission

S. Houshmandyar, M. E. Austin, M. W. Brookman, Y. Liu, W. L. Rowan, and H. Zhao

Citation: [Review of Scientific Instruments](#) **89**, 10H109 (2018); doi: 10.1063/1.5035429

View online: <https://doi.org/10.1063/1.5035429>

View Table of Contents: <http://aip.scitation.org/toc/rsi/89/10>

Published by the [American Institute of Physics](#)

Articles you may be interested in

[Upgrade of the ECE diagnostic on EAST](#)

[Review of Scientific Instruments](#) **89**, 10H111 (2018); 10.1063/1.5035452

[Turbulence measurements on the high and low magnetic field side of the DIII-D tokamak](#)

[Review of Scientific Instruments](#) **89**, 10H106 (2018); 10.1063/1.5036520

[Optimized quasi-optical cross-polarization scattering system for the measurement of magnetic turbulence on the DIII-D tokamak](#)

[Review of Scientific Instruments](#) **89**, 10H107 (2018); 10.1063/1.5035427

[Imputation of faulty magnetic sensors with coupled Bayesian and Gaussian processes to reconstruct the magnetic equilibrium in real time](#)

[Review of Scientific Instruments](#) **89**, 10K106 (2018); 10.1063/1.5038938

[Noise mitigation methods for ion detectors operating with a direct view of high temperature plasmas](#)

[Review of Scientific Instruments](#) **89**, 10I108 (2018); 10.1063/1.5039348

[Instrumentation for the upgrade to the JET core charge-exchange spectrometers](#)

[Review of Scientific Instruments](#) **89**, 10D113 (2018); 10.1063/1.5037639



PFEIFFER VACUUM

VACUUM SOLUTIONS FROM A SINGLE SOURCE

Pfeiffer Vacuum stands for innovative and custom vacuum solutions worldwide, technological perfection, competent advice and reliable service.

[Learn more!](#)

Variable location channels to improve efficiency and precision for direct ∇T_e measurements and high spatial resolution T_e -profile measurements using electron cyclotron emission

S. Houshmandyar,^{1,a)} M. E. Austin,¹ M. W. Brookman,^{1,2} Y. Liu,³ W. L. Rowan,¹ and H. Zhao^{1,3}

¹*Institute for Fusion Studies, The University of Texas at Austin, Austin, Texas 78712, USA*

²*General Atomics, P.O. Box 85608, San Diego, California 92186, USA*

³*Institute of Plasma Physics, Chinese Academy of Sciences, Hefei 230031, China*

(Presented 19 April 2018; received 15 April 2018; accepted 20 June 2018; published online 27 August 2018)

Electron cyclotron emission (ECE) diagnostics that use variable location channels based on yttrium iron garnet (YIG) bandpass filters improve the precision and the efficiency of measurements of electron temperature (T_e) profiles and fluctuations (δT_e). These variable frequency filters were substituted for fixed frequency filters in the intermediate frequency section to achieve the required higher resolution over a target radial range, just before the experiment. Here, we present the proof-of-principle for high temporal resolution measurement of the electron temperature gradient, via real-time slewing of a YIG filter for relocation of an ECE channel during a long pulse. The key component is the application of YIG tunable filters with their narrow bandwidth and capability for a high slew rate of their center frequency. This application permits fast relocation of the ECE channels for direct measurement of the gradient and close spacing of channels to investigate the magnetic island's dynamic behavior. *Published by AIP Publishing.* <https://doi.org/10.1063/1.5035429>

I. INTRODUCTION

Electron cyclotron emission (ECE) diagnostics are the integral to the contemporary tokamaks. Employing narrow bandwidth bandpass filters in the intermediate frequency (IF) section of a radiometer ECE diagnostic increases the spatial resolution of T_e -profile¹ and sensitivity for T_e -fluctuation (δT_e)² measurements. Utilizing yttrium iron garnet (YIG) bandpass filters in the IF section reduces the threshold for the δT_e measurements. The latter is critical to correlational ECE measurements for turbulent transport studies.³ Moreover, the tunable feature of the YIG filters yields the flexibility for moving the ECE channels to regions of interest, even during a discharge. This is noteworthy in the plasma control context as, for example, the fast rearranging of the ECE channels to a rational surface would generate enough information for the actuators to control the neoclassical tearing modes (NTM).

Recently we developed a calibration-free technique⁴ to accurately measure the electron temperature gradient scale length ($L_{Te} = T_e / |\nabla T_e|$). The requirement for that technique is to vary the toroidal magnetic field (B_T) by 1.5% to slew the ECE channels. The measurement is in agreement with the calculation of the gradient scale length from the temperature profile. Moreover, the fine structures in the T_e profiles that are ignored in the common fitting techniques are captured.⁵ Unfortunately, the measurements using this technique suffer from poor time

resolution since rapid modulation of B_T is not possible. Additionally, the B_T variation is not practical for modern tokamaks that employ superconducting magnets. Still the idea of slewing the ECE channels to measure ∇T_e and L_{Te} is advantageous and is achievable by utilizing YIG filters in the IF section.

In this paper, we present the proof-of-principle for real-time ∇T_e measurement via an available YIG filter. The bench testing leading to spatial and temporal resolution characterization of the measurements is discussed in Sec. II. An example of temperature gradient measurements is shown in Sec. III.

II. SPATIAL AND TEMPORAL RESOLUTION OF THE VARIABLE LOCATION ECE CHANNEL

A. Spatial resolution characterization

The YIG filter in use is a custom designed Micro Lambda (MLFP-1652PD) tunable (3.75-18 GHz) YIG bandpass filter, with 3 dB bandwidth of 100 MHz. The filter is fed by a power splitter from the lowest IF band (81-114 GHz) of DIII-D's high resolution fixed frequency channel ECE diagnostic (HRECE).¹ Unlike the previous generations of the YIG filters that would use external voltage to directly drive their tuning coil, setting the frequency of these YIG filters is controlled through application of a 12-bit digital word.

For the purpose of the spatial calibration, an Agilent MXG-N5183A signal generator was used to scan the input frequency to the YIG filter, while the center frequency of the YIG was adjusted with a 12-bit control logic (corresponding to 3.7 MHz per bit step size for the 3.75-18 GHz range) for the YIG which was provided by a National instrument (NI) LabView VI and an NI USB 6003 module. A Schottky diode

Note: Paper published as part of the Proceedings of the 22nd Topical Conference on High-Temperature Plasma Diagnostics, San Diego, California, April 2018.

^{a)}Author to whom correspondence should be addressed: houshmandyar@Austin.utexas.edu

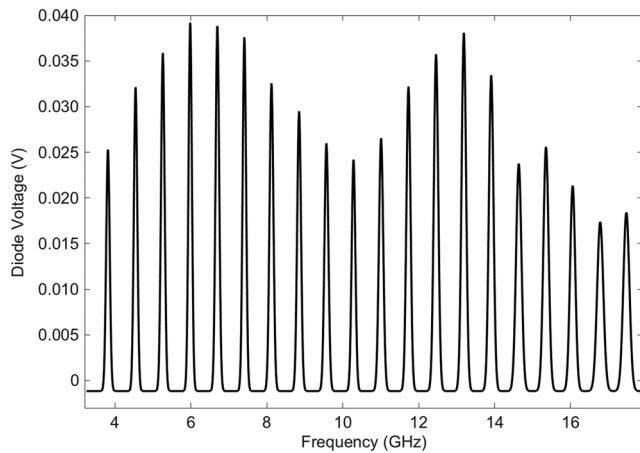
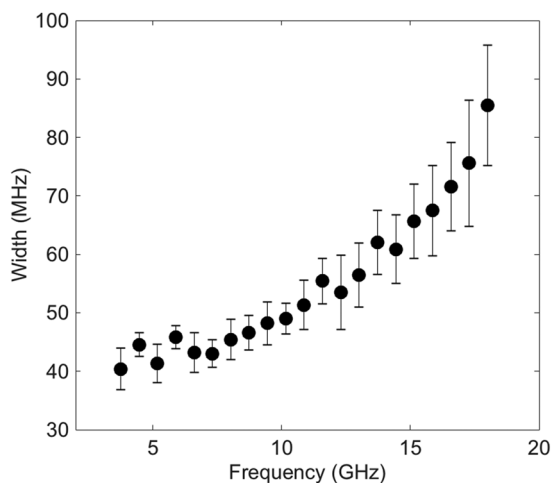
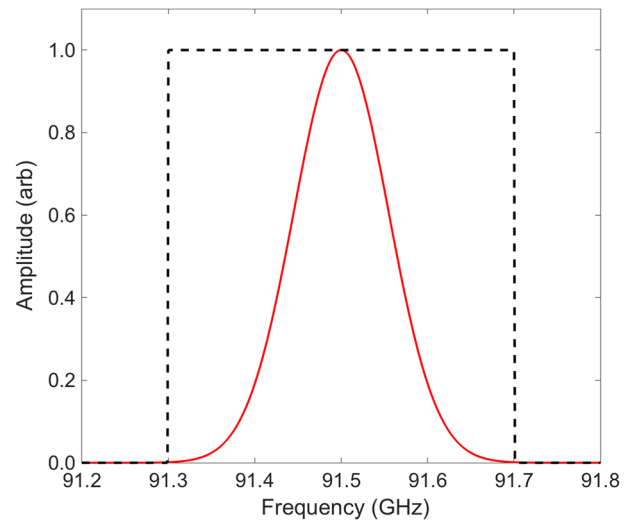


FIG. 1. Frequency response of a YIG bandpass filter.

rectified the output signal of the YIG filter, which was then digitized by the analog input side of the same NI module. For the rest of this paper, the YIG signal refers to the digitized diode's voltage. Figure 1 shows the frequency response (bandwidth and frequency) of the YIG filter when it was set at different frequencies. For each, the responses are characterized with Gaussian fits which was found to capture the bandpass shape. Figure 2 shows the dependence of the variance (σ) of the Gaussian fits on the set frequencies. The information shown in Fig. 2 provides minimum frequency slew (frequency switch) in order to avoid any frequency overlap. In order to have a sense of comparison, Fig. 3 compares the narrow (55 MHz) bandwidth of the YIG filter with the one for a channel of HRECE (400 MHz), when the YIG filter is used as one channel of the IF section.

B. Temporal resolution characterization

Figure 4 shows the lab setup for determining the temporal resolution of the YIG filter when it is slewed. The EC signal was represented by a Noisecom 3208k noise source which provides a continuous and flat RF signal in the 1–18 GHz range; the noise source was connected to the input of the YIG

FIG. 2. Frequency dependence of the Gaussian widths (σ) of the responses shown in Fig. 1.FIG. 3. The bandwidth comparison between the HRECE (dashed line, $\sigma = 400$ MHz) and a YIG bandpass filter (solid line, $\sigma = 55$ MHz) at 91.5 GHz.

filter. Furthermore, the output of the YIG filter was connected to a secondary IF module which consists of a broadband 2–33 GHz low-noise microwave amplifier that provides 20 dB gain. The amplifier is followed by a splitter: each output of the splitter goes through a DC isolation break to prevent inductive pickup and then passes through 6 bandpass filters. The filters are third order Chebyshev type, with a 3 dB bandwidth of 1.5 GHz, with center frequencies at 5.125, 7.375, 9.625, 11.875, 14.125, and 16.375 GHz. A crystal square law detector with 22 GHz bandwidth and 2 V/mW sensitivity converts the power in each channel to a voltage which can be routed to the analog inputs of the NI-USB 6003 module for digitization.

Figure 5 shows the scan of the YIG filter across the center frequencies of the secondary IF module. In order to find the slew rate for switching between any two frequencies within the frequency range of the YIG filter, two channels from the secondary IF module were selected such that the two frequencies would be in the two channels, e.g., $f_1 = 4.7$ GHz in channel 1 and $f_2 = 14.8$ GHz in channel 5 of the secondary IF module. Ultimately, the two channels of the secondary IF module were digitized through the analog input of the NI-USB 6003 unit.

Figure 6 shows an example of a 2-s data acquisition when the YIG filter's frequency was slewed between 4.7 and 14.8 GHz (slew of $\Delta f = 11.1$ GHz), with 250 ms intervals. Since $f_1 (=4.7$ GHz) is only active for the 1st channel of the secondary IF module, the signal from the 1st channel dropped to DC level as soon as the YIG is slewed to $f_2 (=14.8$ GHz). Likewise, since $f_2 (=14.8$ GHz) is only active for the 5th channel of the secondary IF module, the signal from the 5th channel dropped to DC level as soon as the YIG is slewed back to $f_1 (=4.7$ GHz).

The times at which the frequencies are switched are shown as well by recording a transistor-transistor logic (TTL) line. Two different time scales are shown in Fig. 6. Δt_0 is the time that the signal appears momentarily and then disappears, due to overshooting and then undershooting of the current,

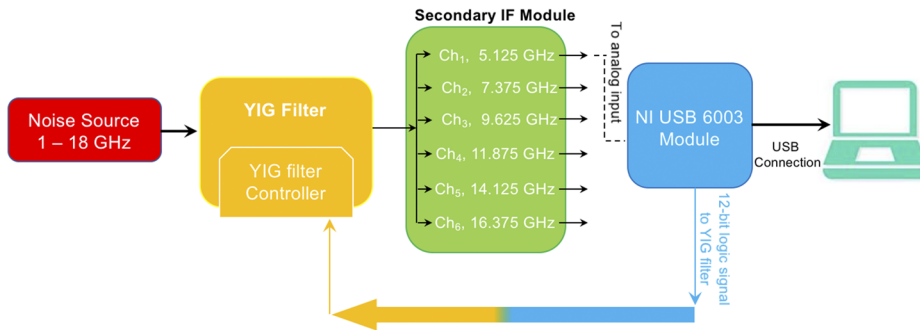


FIG. 4. Experimental setup for slew rate characterization. The center frequencies of the channels of the secondary IF module are identified.

controlled by the YIG’s controller. This effect is known as the “ringing effect” and eventually causes a delay in the settling time scale Δt . Note that the two time scales can be different

in slewing up (f_1 to f_2) or slewing down (f_2 to f_1) cases. Figure 7 shows the slew rates (Δt) as a function of frequency slew. The least square fitting suggests that the slew rates are related to slew frequencies as $\Delta t = (0.47 \pm 0.11) \Delta f + (7.33 \pm 0.71)$, where Δt is in milliseconds and Δf is in GHz units. Therefore, Fig. 7 provides the minimum required time intervals between two slewing frequencies to surpass the ringing effect and the settling time. For example, for 1 GHz slew for electron temperature gradient measurements, 8 ms time interval is required.

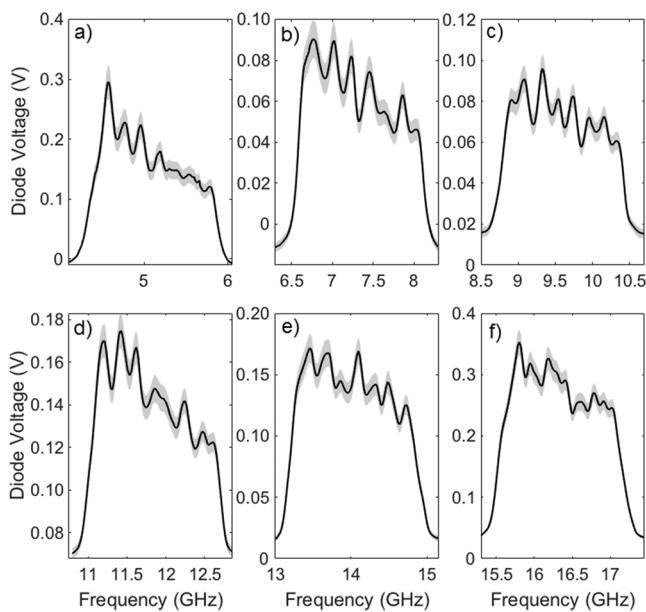


FIG. 5. Frequency response of each channel of the secondary IF module when the YIG filter is scanned across their center frequencies of channels 1 to 6 [(a)–(f)].

III. ELECTRON TEMPERATURE GRADIENT MEASUREMENTS FROM PLASMA

To measure the temperature gradient, the 2-18 GHz split ECE signal from the 81 GHz local oscillator (LO) of the HRECE was fed to the YIG filter; the output voltage from the schotky diode was digitized at 500 kHz. Two frequencies of $f_1 = 6.5$ GHz and $f_2 = 7.5$ GHz were selected for frequency slew at 15 ms intervals. The two frequencies correspond to the frequencies of channels 5 and 6 of HRECE which have center frequencies of 87.5 and 88.5 GHz. This frequency selection will allow the calibration of YIG filter’s signals at their set frequencies and hence ∇T_e measurements during a plasma discharge.

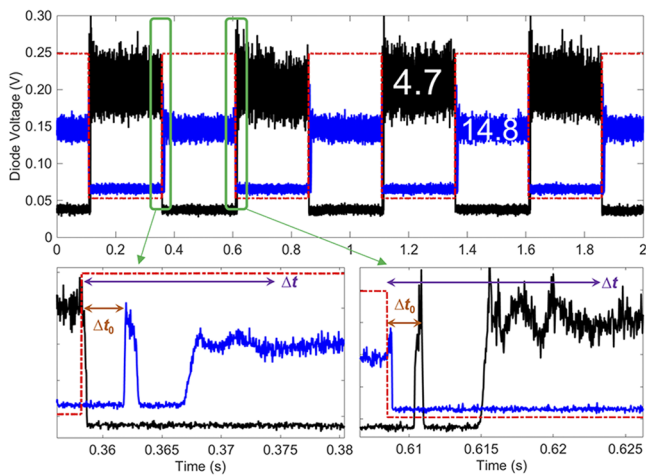


FIG. 6. Time response of the YIG filter when slewed between two frequencies at 4.7 and 14.8 GHz. The time scales for the ringing effect (Δt_0) and settling time (Δt) are identified. The red dashed line represents one TTL line where TTL-high (scaled) and TTL-low correspond to 14.8 GHz and 4.7 GHz, respectively.

Figure 8 shows the plasma parameters as a function of time for a DIII-D tokamak discharge, including the electron temperature for channels 5 and 6 of HRECE. As it is indicated in Figs. 8(c) and 8(d), the sawtooth features (and perhaps

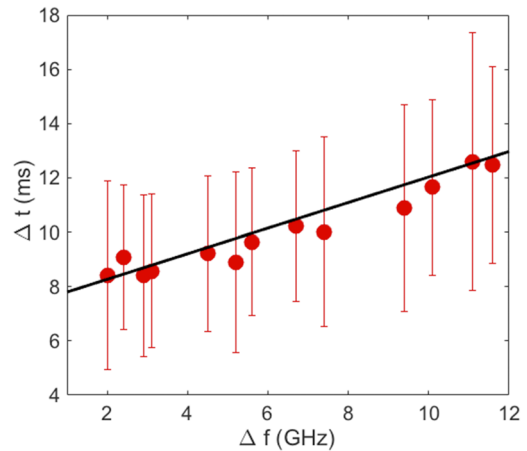


FIG. 7. Settling time as a function of frequency slew.

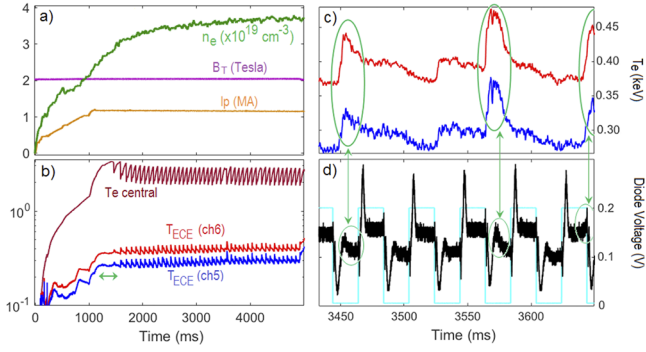


FIG. 8. Time evolution of a DIII-D discharge (a) and (b), used for gradient measurements using the YIG filter. The center frequencies of channels 5 and 6 of HRECE (c) are consistent with the slewing frequencies of the YIG filter (d). The effects from the sawteeth are identified. The TTL trace is shown in plot (d), where TTL-high (scaled) and TTL-low correspond to 7.5 GHz and 6.5 GHz, respectively.

other MHD instability features in the ECE signals) and the ringing effects need to be excluded from the slewed YIG filter's signal before the signal can be used for the gradient measurements.

To accomplish the absolute calibration, a period without sawteeth is selected, as shown in Fig. 8(b) with an arrow and zoomed in Fig. 9. The ratio of the electron temperature for channel 5 ($TECE_5$) to the average YIG filter's signal set at 6.5 GHz (ECE_1) is the calibration factor. Furthermore, the ratio of the YIG filter's signal during the slew, i.e., $ECE_2/ECE_1 = 0.147/0.105 = 1.4$, is in good agreement with the temperature ratio of the HRECE's channels 5 and 6, i.e., $TECE_6/TECE_5 = 1.33$. Thus, by knowing the calibration and hence the change temperature (ΔT_e) and frequency slew Δf , the electron temperature gradient ($\nabla T_e \approx \Delta T_e/\Delta R$) can be measured in real time. Here, $\Delta R = R_0 \Delta f/f_0$, where R_0 is the viewing

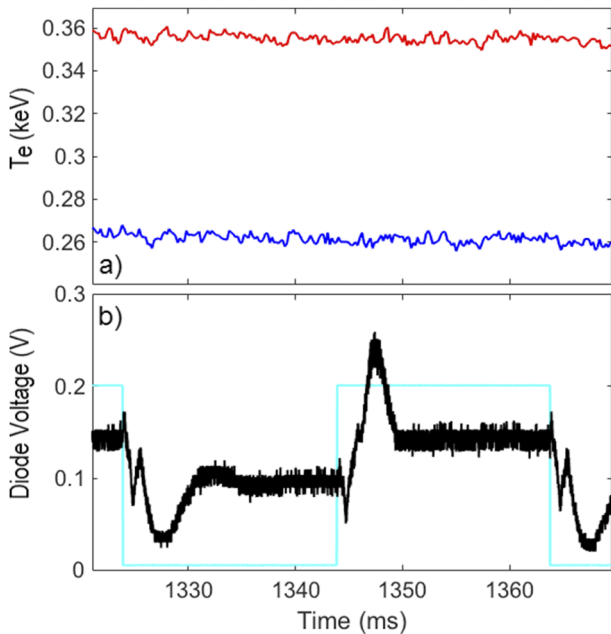


FIG. 9. The sawtooth-free section of the discharge [shown in Fig. 8(b)] is chosen for the YIG's signal (b) calibration with reference to channels 5 and 6 of HRECE (a).

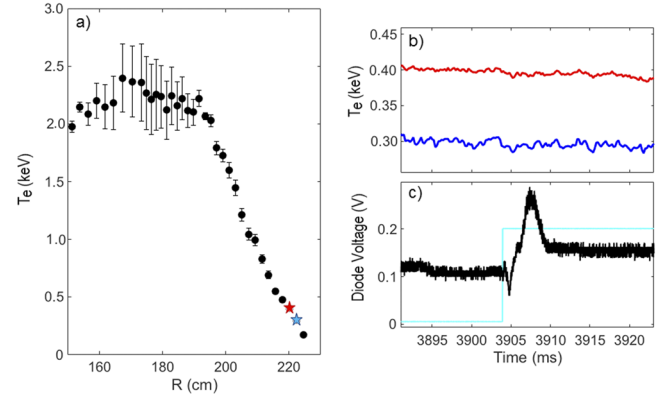


FIG. 10. Electron temperature versus major radius, measured by HRECE, averaged between 3890 ms and 3920 ms of the discharge (a). Channels 5 and 6 are identified with blue and red stars, respectively. The electron temperature for channels 5 and 6 (b) and the signal from the YIG filter (c) for the same time interval.

of the ECE channels with f_0 (sum of the local oscillator's and YIG's frequencies, $f_{YIG} + f_{LO}$) frequency. Note that ΔR can also be determined using EFIT equilibrium information.

However, it is the electron temperature gradient scale (L_{Te}) that plays the important role in turbulent transport narrative and the scale length can be found directly from the slewed YIG's signal without the knowledge of the calibration since $L_{Te}^{-1} = (\Delta R \times ECE_i/\Delta ECE)^{-1}$. Here ECE_i is the ECE value before the slew, and ΔECE is the change in the ECE due to the slew. Using this equation, the inverse scale lengths are calculated to be 16.8 m^{-1} and 20.9 m^{-1} for the slew-up and slew-down times, respectively.

The electron temperature profile from HRECE is shown in Fig. 10, with channels 5 and 6 identified. Using the temperatures and the location of the two channels yields $\nabla T_e = \Delta T_e/\Delta R = -(4.62 \pm 1.7) \text{ keV/m}$ and $L_{Te}^{-1} = -\nabla T_e/T_e = 13.6 \pm 5.1 \text{ m}^{-1}$. This number is in agreement with the one found from the calibration-free scheme.

IV. SUMMARY AND FUTURE DESIGN

Here we have used a state-of-the-art yttrium iron garnet (YIG) bandpass filter and developed a technique to measure the time evolution of the electron temperature gradient scale length ($L_{Te} = T_e/|\nabla T_e|$) and the electron temperature gradient (∇T_e) by rapidly slewing the YIG filter. Since the YIG filter in-use is not designed for fast frequency slew, the ringing effect and long settling times limit the temporal resolution of the gradient measurements. A new set of YIG bandpass filters are in the design process to reduce the settling time to $600 \mu\text{s}/\text{GHz}$ (slew frequency). These filters will have sophisticated windings to avoid high inductance and hence avoid ringing effects.

The fast frequency slew feature of the filters provides new capabilities and innovative plasma diagnostics. For example, monitoring magnetic island dynamics can be achieved with these YIG filters. Here are some practical schemes for this monitoring: (a) a single filter can be slewed across the island region in an effort to search for two minima (i.e., x-points) and (b) a cluster of filters can be located within the island

region to search for flattening in T_e at the rational surfaces and/or measure ∇T_e and/or $L_{T_e}^{-1}$ (as described in Sec. III) to search for their minimum at the rational surfaces. Additionally, a phase comparison among the channels of the cluster identifies the island.

Future experiments include employing these fast slew YIG bandpass filters in the IF section of an existing radiometer at the EAST tokamak with a 90 GHz local oscillator. For an EAST discharge at $B_T = 2$ T, the combination of the local oscillator's frequency and the YIG filter's frequency range yields resolving the T_e -profile from pedestal to the $q = 1.3$ rational surface. This combination can potentially provide a predictive

scheme to avoid locked modes by measuring the island size and location, right before the locked mode event.

ACKNOWLEDGMENTS

This work was supported by the U.S. Department of Energy OFES, under Award Nos. DE-FG02-97ER54415 and DE-SC0010500.

¹D. D. Truong *et al.*, *Rev. Sci. Instrum.* **85**, 11D814 (2014).

²M. Fontana *et al.*, *Rev. Sci. Instrum.* **88**, 083506 (2017).

³M. Fontana *et al.*, *Nucl. Fusion* **58**, 024002 (2018).

⁴S. Houshmandyar *et al.*, *Rev. Sci. Instrum.* **87**, 11E101 (2016).

⁵S. Houshmandyar *et al.*, *Phys. Plasmas* **25**, 042305 (2018).